Struct Multidisc Optim (2018) 57:1357–1375
DOI 10.1007/s00158-017-1817-y

INDUSTRIAL APPLICATION

Design optimization of aircraft landing gear assembly under dynamic loading

J. Wong[1] · **L. Ryan**[1] · **I. Y. Kim**[2]

Received: 5 June 2017 / Revised: 2 August 2017 / Accepted: 14 September 2017 / Published online: 30 September 2017
© Springer-Verlag GmbH Germany 2017

Abstract Aircraft landing gear assemblies comprise of various subsystems working in unison to enable functionalities such as taxiing, take-off and landing. As development cycles and prototyping iterations begin to shorten, it is important to develop and improve practical methodologies to meet certain design metrics. This paper presents an efficient methodology that applies high-fidelity multi-disciplinary design optimization techniques to commercial landing gear assemblies, for weight, cost, and structural performance by considering both structural and dynamic behaviours. First, a simplified landing gear assembly model was created to complement with an accurate slave link subassembly, generated based of drawings supplied from the industrial partner, Safran Landing Systems. Second, a Multi-Body Dynamic (MBD) analysis was performed using realistic input motion signals to replicate the dynamic behaviour of the physical system. The third stage involved performing topology optimization with results from the MBD analysis; this can be achieved through the utilization of the Equivalent Static Load Method (ESLM). Lastly, topology results were generated and design interpretation was performed to generate two designs of different approaches. The first design involved trying to closely match the topology results and resulted in a design with an overall weight savings of 67%, peak stress increase of 74%, and no apparent cost savings due to complex features. The second design focused on manufacturability and achieved overall weight saving of 36%, peak stress increase of 6%, and an estimated 60% in cost savings.

Keywords Topology optimization · Equivalent static load method · Multi-body dynamics · Aerospace · Aircraft landing gear

✉ J. Wong
jon.wong@queensu.ca

L. Ryan
luke.ryan@queensu.ca

I. Y. Kim
kimiy@queensu.ca; http://me.queensu.ca/People/Kim/

[1] Department of Mechanical and Materials Engineering, Queen's University, Room 213, Jackson Hall, 5 Field Company Ln, Kingston, ON K7L 2N8, Canada

[2] Department of Mechanical and Materials Engineering, Queen's University, Room 305, McLaughlin Hall, Kingston, ON K7L 3N6, Canada

1 Introduction

1.1 Background and motivation

As our world continues to grow and interact with one another in a global sense, there will be a subsequent increase in demand for aviation as the mode of transportation to accommodate these growths. The International Air Transport Association (IATA) forecasts a doubling of annual air travelers over the next 20 years from approximately 3.8 billion passengers in 2016 to 7.2 billion in 2035 (International Air Transport Association 2016a). In order to meet these demands, airline companies will need to increase their fleets of aircraft in order to expand their network of operations. Although the rise of these demands continue to incur, it is also equally important to consider the environmental impacts of increased aviation. To offset these impacts, IATA has set a target of an average improvement of 1.5% in fuel efficiency per year from 2009 to 2020 (International Air Transport Association 2016b). The use of lightweight design techniques on aircraft components may be utilized to improve fuel efficiency. It has been shown that for 10 kg of weight savings, 3925 kg of fuel and subsequently 4 tons of CO_2 can be saved (Deveau 2013).

Aircraft landing gear systems are composed of numerous mechanical and structural components interconnected together to enable movement while on the ground and are stowed away within the aircraft while in flight to reduce drag and improve aerodynamic efficiency. Due to weight and space limitations, few redundancy systems exist within landing gear systems. However, they must endure the extreme impact and vibrational loading experienced during landing and braking, and are consequently deemed critical components. Therefore, it is imperative that these components are designed with a high degree of robustness and reliability. As the aerospace industry continues to shorten their development cycles and prototyping iterations while setting more ambitious cost and weight targets, it is important to develop and improve practical methodologies to meet these growing demands.

In terms of landing gear design, the two primary loading cases that are typically considered are vertical loading induced when the tire comes into contact with the ground during landing and fore/aft loading which occurs when brakes are applied to decelerate an aircraft upon landing. However, another important consideration that is also of high importance in design is that there are also induced vibrational loads as a result of the aforementioned loading and can be classified by two possible phenomena: "shimmy" and "gear walk". These vibrational loads have the tendency to cause limit cycle oscillations and may cause additional mechanical wear at the joints or interface of various components that have been excited.

Shimmy is a generic term used to describe self-induced oscillations about the vertical axis of the landing gear strut. Typically, as a result of lateral bending and torsion, shimmy is considered a type of vibrational loading, which can occur in various conditions such as during taxiing, take-off as well as landing. Similarly, gear walk is another phenomenon that is used to describe oscillations in the fore/aft direction of the landing gear, and this typically occurs during landing impact or braking. In many instances, it is possible to have both shimmy and gear walk coupled and the factors that contribute to these phenomena include elasticity in the landing gear components, variability in tire pressure and contact patch of different wheels, friction and free-play of pinned joints.

There are various configurations of landing gear layouts, but the tricycle layout is one of the most common configurations used in modern aviation, as they offer a high level of stability and maneuverability. Typically, tricycle landing gears are composed of a single nose landing gear (NLG) and two sets of main landing gears (MLG) located in line with the wings of an aircraft. Within each of these nose or main landing gear assemblies are various subassembly mechanisms that enable various functionalities. For instance, the shock absorber connected to the main strut acts as a spring-damper mechanism to soften vertical loading experienced during landing. The torque-link subassembly provides the landing gear with torsional stiffness to prevent twisting between the main strut and the lower wheel assembly. The landing gear retraction mechanism allows for storage within the fuselage or wing, and is enabled by components such as the side and drag strut along with various actuators.

Although the dynamics of each mechanism independently is well understood, the coupling and interactions between multiple mechanisms creates complexities in modeling and analysis. To add to these complexities, structural performance is a crucial aspect to consider in the design of landing gears to ensure components are able to withstand various time-dependent loading conditions. The coupling of dynamic and structural analysis is inherently a difficult problem to solve due to the number of nonlinearities introduced as well as the increased computational cost involved with considering multiple components. Once this behavior has been accurately characterized, various optimization techniques can be used to improve weight, cost, and performance of the part.

1.2 Literature study

The dynamics of aircraft landing gears have been studied extensively and there are a number of notable publications. For instance, mathematical models using rigid body assumptions were developed to simulate how landing gears behave when maneuvering on the ground and validated through various experimental testing (Hitch 1981). Other notable overviews in regards to aircraft ground simulation include publications by AGARD (1995) and Besselink (2000), which focus more heavily on accurate simulations of the shimmy phenomenon, and Krüger et al. (1997), which discusses various numerical modelling approaches to simulate various ground operation scenarios, shimmy, and touch down dynamics. A number of modeling techniques proposed by Denti and Fanteria (2010) and Tadeusz et al. (2006) have been utilized to accurately capture the effects of wheel ground contact and the corresponding response. A literature survey conducted by Pritchard (2001) summarizes the work that has been done in the past with regards to analytical, experimental, and some computational modeling of landing gear dynamics.

The multi-body dynamic (MBD) analysis of various landing gear mechanisms is another important area of research to consider. A single-sidestay mechanism was successfully modelled using numerical continuation analysis and a rigid-body assumption in an article published by Knowles et al. (2013). As previously mentioned, however, vibrational loading is a highly important loading scenario to consider in landing gear design. It is desirable to model components as deformable bodies, rather than rigid bodies, because the behavior of these oscillations are affected by the elasticity of the landing gear frame. This has been shown to be case in another article published by Krüger and Morandini (2014), which discussed the differences in the stability simulated responses for a various landing gear components modeled with rigid and

flexible components under oscillating phenomenon such as shimmy and gear walk.

In terms of structural analysis of landing gear components, the majority of the work that has been done involves simply translating loads obtained from dynamic analysis into approximate static forces and pressure distributions. A nose landing gear structural analysis was conducted by Nguyen et al. (2012) with static loads derived through analytical kinematics and Federal Aviation Administration (FAA) standards. A similar analysis was done by Gowda and Basha (2014), who also conducted a structural analysis on another nose landing gear design as well as a subsequent fatigue analysis. A dual locking linkage mechanism was carefully modelled by Oh (2014) and the kinematic analysis was performed in ADAMS, to which they used obtain static tension and compression loads to apply to the linkage component.

In order to fully utilize the available design freedom when optimizing existing designs to reduce cost and weight, topology optimization is typically used to yield the most benefits. Typically done with linear static load cases, topology optimization is not be readily applicable for landing gear systems because of the complexities that come from dynamic loading and interaction between various components. This has the potential to lead to suboptimal results, as the load cases used to describe the behavior of the system may not be accurate. Although the alternative is to conduct a fully nonlinear topology optimization, this is an undesirable technique to use because it is computationally very expensive to the point where it is not practical. Topology optimization with geometric and material non-linearity has been done with some success but only for simple test case geometries (Lee and Park 2012).

Alternatively, a method that has been proven successful in various simple problems and even some practical problems in other industry is the use of equivalent static load method (ESLM). The methodology behind ESLM has been described in the works of Choi et al. (2005) and Park (2011), with applications in various fields as outlined in Kang et al. (2001), Li et al. (2014) and Sun et al. (2016). Other than a white paper published by Altair Engineering on the potential to utilize this technique for landing gear systems without concrete methodologies and results (2008), there has been no mention of any landing gear components optimization that considered MBD and topology optimization.

As cost and weight targets for landing gear increase at an aggressive rate coupled with the demand for shorter development cycles, new approaches must be explored in order to generate designs for real world applications in an accurate yet efficient manner. For instance, this approach must be able to take into consideration the coupling of both multi-body dynamics and structural loading aspects directly within the analysis process and subsequently used in optimization.

The objective of this paper is to develop and perform high-fidelity multi-disciplinary design optimization of commercial landing gear assemblies for weight, cost, and structural performance by considering structural and dynamic behaviours. Specifically, a slave link subassembly will be selected as the candidate to explore the feasibility of this methodology. The components considered are tertiary, which do not require expensive and time-consuming recertification testing in order to be put into service and thus have a greater potential of being implemented, if proven successful. Their sole purpose is to guide secondary hydraulic and electrical lines from the upper landing gear to the wheel hub. The design optimization problem statement for the design process is presented in Section 2. Section 3 includes the process of converting CAD files into a meshed assembly, along with advanced modeling techniques for accurate modeling of component joints and design domain setup for topology optimization. Next in Section 4, an MBD analysis with flexible bodies is performed on the slave link assembly. The resultant time-dependent deformations from the MBD analysis is converted, through ESLM, into multiple load cases from specific time steps that will be used to conduct topology optimization for various components in Section 5. Several results were obtained by altering various optimization parameters and constraints to drive the solution towards a more effective design. Once results are generated, the most effective topology is selected for a detailed design interpretation in Section 6 and ultimately validated against the baseline in Section 7. Altair Hypermesh was the software used for finite element modeling, while Optistruct was used to conduct the MBD analysis with flexible bodies as well as a subsequent topology optimization with ESLM.

2 Mathematical problem statement

The design optimization problem of the slave link assembly components can be described with the following mathematical statement:

$$\begin{aligned} &\textit{minimize} \quad C\left(\rho_i^{(k)}\right) \\ &\textit{subject to} \begin{cases} K_L\left(\rho_i^{(k)}\right) U_L^t = f_{eq}^t \\ \sum_{i=1}^{N} \rho_i^{(k)} v_i - V^* \le 0 \\ 0 < \rho_{min} \le \rho_i^{(k)} \le 1 \\ \rho_i^{(k)} = g_j(d_i) \end{cases} \end{aligned} \tag{1}$$

where the objective is to minimize the compliance C under dynamic loading, ρ_i represents the element density of the i-th design variable d_i for topology optimization. k identifies the optimization outerloop iteration, which is explained further in Section 5.3. U_L^t and f_{eq}^t are nodal displacement and equivalent static loads vectors at time step t, respectively, and K_L is the linear global stiffness matrix. V^* denotes the volume fraction constraint, and v_i is the

element volume of the *i*-th design variable. ρ_{min} is the minimum allowable density to prevent the occurrence of numerical instabilities in the optimization. Lastly, g_j represents the *j*-th manufacturing or symmetry constraint function imposed on the design space to drive the optimal solution towards a more readily manufacturable result. An optimization process overview is shown in Fig. 1.

3 Computational modeling

3.1 CAD modeling and simplifications

CAD drawings for various components of the slave link assembly were giving and then modeled using SolidWorks.

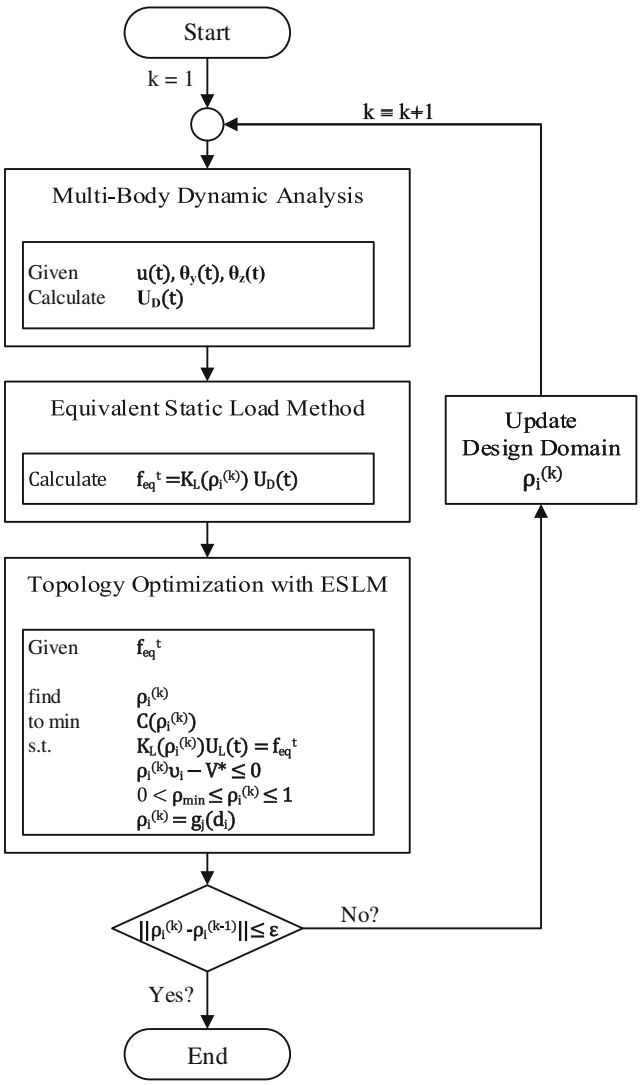

Fig. 1 MBD Topology Optimization Process Overview. Symbols and variables are explained in (1) for Topology Optimization with ESLM, (2), (5), and (6) for Multi-Body Dynamic analysis, and (9) for Equivalent Static Load Method. ε represents the optimization convergence criterion

Specifically, the two main components that were to be optimized in the design process include the upper slave link and lower slave link.

The slave links are manufactured from 7000-series aluminum. As previously mentioned, the primary purpose of these two linkage components are to act as cable guides for secondary hydraulic and electrical lines. Attached to the linkage components are Delrin cable guides, which come into direct contact with the cable lines and provide less sliding friction when the landing gear is in motion.

In terms of joint connections, the upper slave link is connected to the upper strut through a revolute joint, a ball joint between the upper and lower slave link, and universal joint to connect the lower slave link to the lower strut. This joint configuration was selected to allow the mechanism to have the necessary degree of freedoms to accommodate for the vibrational loading present. The material used to model the pin connections is stainless steel.

To save on computational modeling resources, the upper and lower strut CAD geometries were simplified significantly, as they were not the main focus of this research. To ensure the behavior of the slave link assembly will behave in a similar manner with the physical system, the location for the upper and lower strut connection point were kept consistent. The entire assembly is shown in Fig. 2. Note that the secondary lines were modeled for visualization purposes only.

3.2 Finite element modeling

A finite element model was created from the geometries in the CAD assembly model. The entire meshed model of the slave link assembly and landing gear test rig is found in Fig. 3 and is composed of approximately 535,000 finite elements and 861,000 nodes. The top grey block acts as a grounding point for the multi-body dynamic model and represents the point of connection for the landing gear to the aircraft frame.

In order to define joints with specific degree of freedoms enabled to replicate the correct motion, two coincident nodes, one from each component being attached, must be created and linked. There are various techniques to attach joint nodes to components with different advantages and disadvantages. The simplest and most computationally efficient technique for joining is to use rigid (RBE2) elements between the joint node (independent) and the nodes on the inner faces of the hole to which a pin would slot in (Fig. 4-A). The disadvantage to this technique is that it over-stiffens the joint and leads to inaccuracies in the subsequent results. An alternative technique is to use solid elements within the pinholes and connect the rigid elements to the face of the solid elements. The solid elements can then be given material properties to match that of the physical pins and allows for small deformations of the pin to be captured by the model (Fig. 4-B). The disadvantages are that this approach is more computationally costly than just

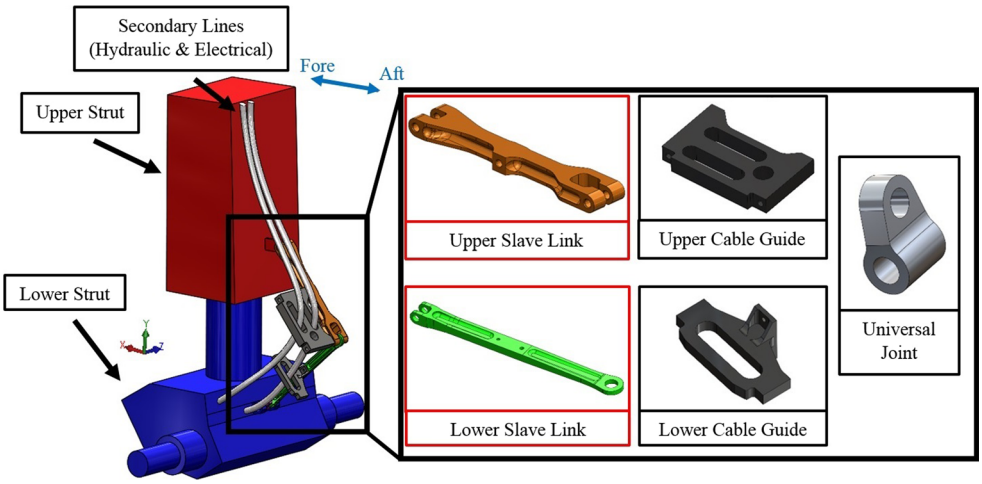

Fig. 2 Slave link assembly components on a simplified landing gear. Design optimization is applied to the upper slave link and lower slave link

using rigid elements, and there are still some slight inaccuracies present. For instance, when the pin is under bending, one side of the pin experiences compression loading due to contact with the component. As a result of the solid element mesh being connected with the component elements, however, the opposite side of the pin experiences an artificial tension loading equal to the compression. A technique to prevent this from occurring is to introduce contact elements between the solid pin elements and the corresponding mating hole (Fig. 4-C). This will improve the accuracy of the result; however, the computational cost for running the model will also increase. With the number of different joints present in the model, contact elements may also introduce numerical instabilities.

Since the end purpose of this model is to conduct topology optimization, solid pin elements were utilized as the technique for connecting joint nodes to components because they provide sufficient levels of accuracy without adding a substantial amount of computational cost.

Once the joints were modelled with solid pin elements, joint definitions were prescribed to each joint in a manner, which matched the physical system. To enable the landing test rig to experience gear walk, a revolute joint (J1) was imposed between the upper strut and the fixed ground block to allow for a pivot motion about the Z-axis. Similarly, a cylindrical joint (J2) was given to the connection between the upper and lower strut to provide the necessary degrees of freedom (D.O.F.) for the shock

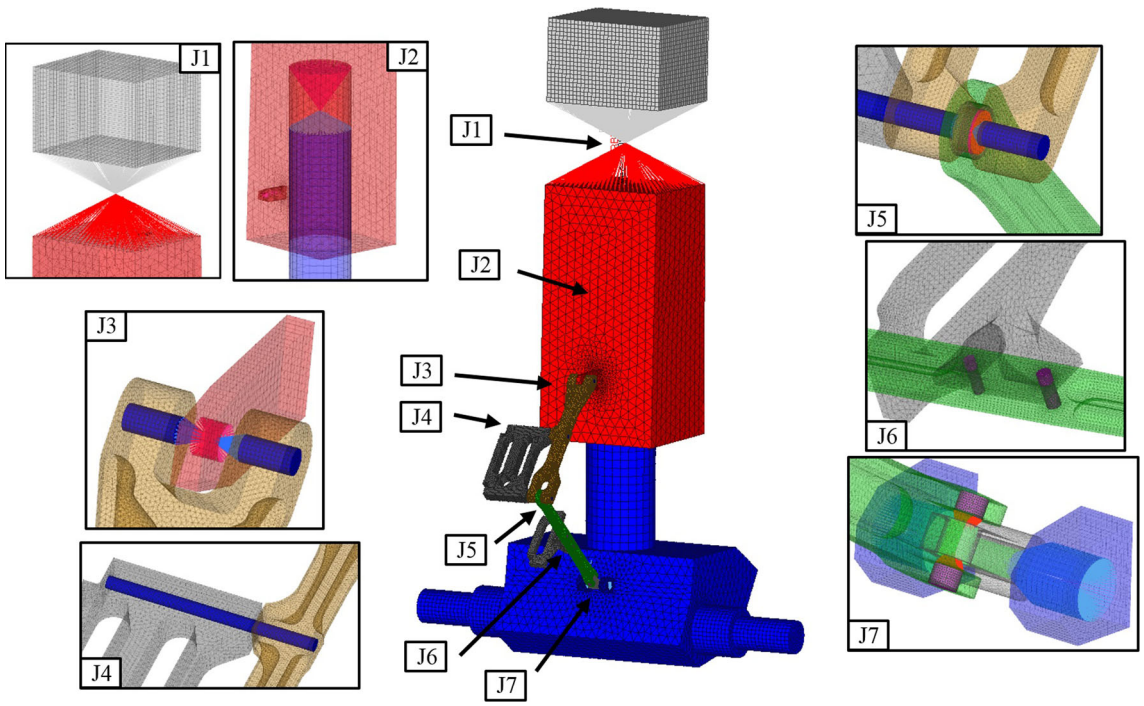

Fig. 3 Finite element model of slave link assembly on simplified landing gear test rig

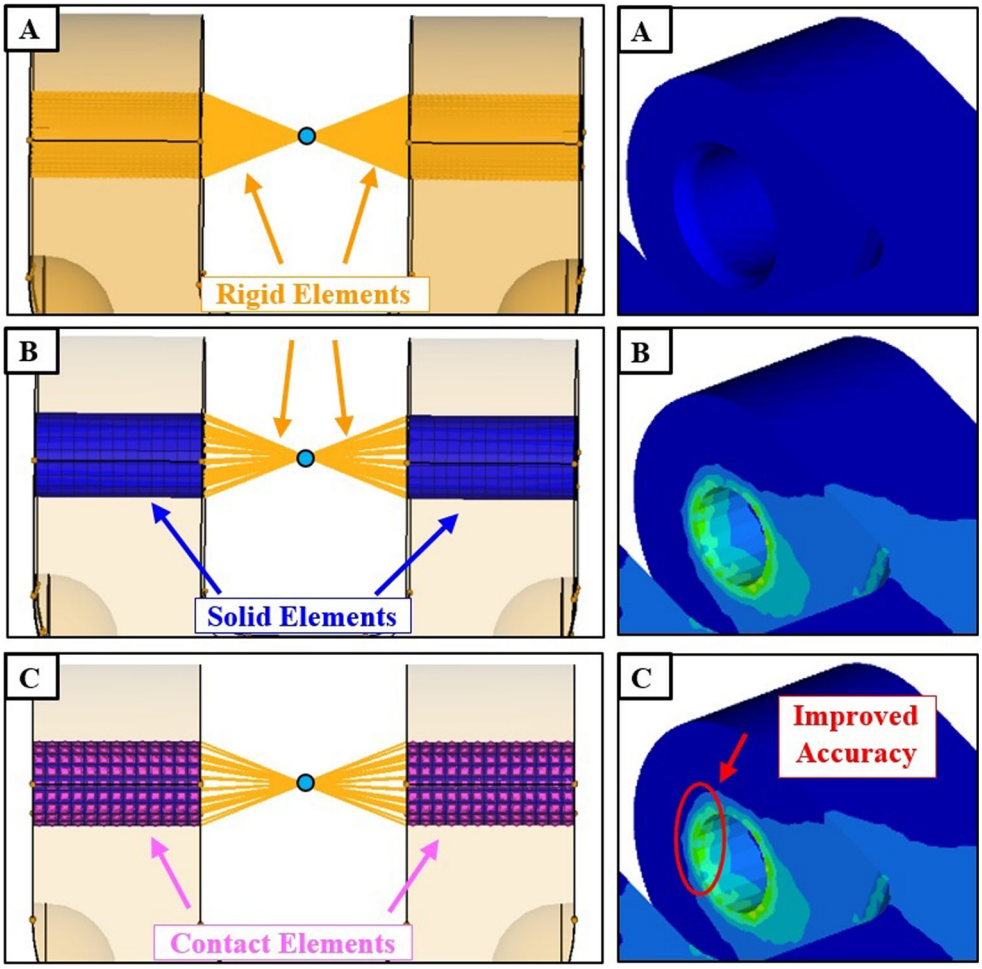

Fig. 4 Joint modeling techniques and effects on analysis

absorber compression and shimmy motion. Based on the drawings of the physical system, the following joint definitions were prescribed: a revolute joint (J3) between the upper strut and upper slave link, a ball joint (J5) between the upper slave link and lower slave link, and a two revolute joints (J7) to replicate a universal joint where the two axis of rotations are offset from one another to connect the lower slave link to the lower strut. The connection between the cable guide and slave link for both upper (J4) and lower (J6) were modelled using solid pin elements with no D.O.F. The joint definitions are summarized in Table 1.

The next step in the modeling of the landing gear assembly is to define the body types of each component in the system. For an MBD analysis, there are three possible body definitions to prescribe: ground, rigid, and flexible. The ground definition was set to the ground component and remained fixed throughout the analysis. Rigid body definition was given to the upper and lower strut as their main purpose in the analysis is to transmit the input motion experienced during a landing load case into the slave link assembly and there is no interest in the structural behavior of these simplified components. The rest of the components, which include the slave links, cable guides, universal joint, and pins, were given a flexible body definition, as the structural aspects of these components will be analyzed. Table 2 and Table 3 summarizes the body definitions for each component in the finite element model, along with their corresponding material composition.

Material properties for steels and aluminum used in this model were obtained from ASM Handbooks (Schmidt and Rohrbach 1990) while the properties for the Delrin plastic were obtained from a supplier's datasheet (DuPont 2016).

4 Multi-body dynamics with flexible body

4.1 Analysis parameters

Improvements in computing power and methods have given rise to techniques that now exist to couple MBD and structural analysis through flexible elements. Techniques for deformable MBD modeling and simulation outlined in publications by Shabana (1997), Bauchau (2011) and Cardona (2000) have been implemented in modern FE software packages with practical example results from Xingguo et al. (2007). Although

Table 1 Component joint definitions

ID	Component 1	Component 2	Joint Type	Rotational D.O.F.	Translational D.O.F.
J1	Ground (Fixed)	Upper Strut	Revolute	1	0
J2	Upper Strut	Lower Strut	Cylindrical	1	1
J3	Upper Strut	Upper Slave Link	Revolute	1	0
J4	Upper Cable Guide	Upper Slave Link	Solid Pin	0	0
J5	Upper Slave Link	Lower Slave Link	Ball	3	0
J6	Lower Cable Guide	Lower Slave Link	Solid Pin	0	0
J7	Universal Joint	Lower Slave Link	Revolute	1	0
J7	Universal Joint	Lower Strut	Revolute	1	0

these concepts have existed for some time, no work has been performed for landing gear slave link systems.

Before conducting an MBD analysis, various types of motion experienced by a landing gear were carefully studied and characterized. The findings led to the definition of three input motions that would lead to replicating the behavior of the physical system. The first motion involves the translational motion of the lower strut because of the shock absorber compressing upon landing. The second and third motion involve vibrational loads induced on the system during landing such as shimmy and gear walk. To replicate these phenomena, a rotational motion about the Y-axis is prescribed to the lower strut in place of shimmy and a rotational motion about the Z-axis is prescribed between the upper strut and the ground block (Fig. 5).

The translational motion $u(t)$ of the lower strut can be described mathematically with the following second order response equation:

$$u(t) = A_1{}^{*}\left[1-\frac{1}{\beta}e^{-\zeta_1(2\pi f_1)t}sin(2\pi f_1\beta t+\alpha)\right] \tag{2}$$

$$\beta = \sqrt{1-\zeta_1{}^2} \tag{3}$$

$$\alpha = cos^{-1}\zeta_1 \tag{4}$$

where t denotes the time-domain, A_1 represents the final compressed position of the lower strut, f_1 is the frequency at which the response occurs, ζ_1 is the damping ratio.

For the rotational shimmy $\theta_y(t)$ and $\theta_z(t)$ gear walk motion, a mathematical equation for decaying oscillations was used and are as follow:

$$\theta_y(t) = A_2e^{-\zeta_2(2\pi f_2)t}\sin(2\pi f_2t) \tag{5}$$

$$\theta_z(t) = A_3e^{-\zeta_3(2\pi f_3)t}\sin(2\pi f_3t) \tag{6}$$

where A_2, A_2 are the amplitudes of oscillation, ζ_2, ζ_3 are the damping ratio, and f_2, f_3 are the frequency of oscillation.

Based on a review of findings from AGARD (1995) and Besselink (2000), parameter values for the input motion were determined and shown in Table 4, along with plots shown in Figs. 6 and 7.

4.2 Flexible body generation and MBD results

Transient Multi-Body Dynamic (MBD) analysis is performed using OptiStruct 14.0 (2015a). The MBD solver within OptiStruct utilizes a combination of Differential Algebraic Equation (DAE) integrator (Brenan et al. 1996) and Backward Differentiation Formula (BDF) method to solve the Euler-Lagrange representation of the equations of motion (2015b) and a simplified version for explanation purposes is represented as follow:

$$M\ddot{U}_D + \Phi_x^T\lambda - f\left(U_D, \dot{U}_D\right) = 0 \tag{7}$$

$$\Phi(U_D, t) = 0 \tag{8}$$

Table 2 Material properties for components modeled

Material	Density [kg/m^3]	Poisson's Ratio [–]	Young's Modulus [GPa]	Yield Strength [MPa]
AISI 4340 M Steel	7750	0.30	210	1586
Al-7075-T73XXX	2830	0.33	72	435
17-4PH Stainless Steel	7750	0.30	190	1172
Delrin 100 NC010	1420	0.35	3.1	72

Table 3 Body definition for MBD Analysis

Component	Material	Body Type
Ground (Fixed)	N/A	Ground
Upper Strut	AISI 4340 M	Rigid
Lower Strut	AISI 4340 M	Rigid
Upper Slave Link	Al-7075-T73XXX	Flexible
Lower Slave Link	Al-7075-T73XXX	Flexible
Upper Cable Guide	Delrin 100 NC010	Flexible
Lower Cable Guide	Delrin 100 NC010	Flexible
Universal Joint	Al-7075-T73XXX	Flexible
Joint Pins	17-4PH H1025 SS	Flexible

Table 4 Parameter values for input motion

Variable	Value	Units
A_1	200	[mm]
f_1	1	[Hz]
ζ_1	0.70	[−]
β	0.7141	[−]
θ	0.7954	[−]
A_2	2.5	[deg]
f_2	30	[Hz]
ζ_2	0.01	[−]
A_3	0.1875	[deg]
f_3	30	[Hz]
ζ_3	0.01	[−]

where M represents the mass matrix, Φ is the displacement constraints vector, f is the external force vector, λ are the Lagrange Multipliers, and $U_D, \dot{U}_D, \ddot{U}_D$ are the calculated displacement, velocity, and acceleration vector. Note that these equations meant to serve as a high level overview and detailed information is available from Altair (2015b). This solver was selected because it is robust and computationally efficient.

To introduce flexible bodies into the analysis, component mode synthesis (CMS) is performed on the finite element model to reduce the modal stiffness of the body to include only the joint interface degrees of freedom and a set of normal modes (2015b). The normal modes and reduced modal stiffness for each flexible body was obtained using the Craig and Bampton method (1968).

The MBD analysis was conducted on a Windows workstation PC (Intel i7-5820 k, 12 cores 4.0 GHz, 65,431 MB DDR4 RAM 2133 MHz), and the CPU time was 0.95 h. The outputs of the analysis can be categorized into dynamic and structural behaviors. These results are shown in Fig. 8.

To examine the dynamic behavior, displacement and acceleration plots for the upper and lower slave link at their corresponding center of gravities was generated. Based on these results, it can be seen that the upper and lower slave link exhibit different response behaviors in regards to which vibrational motion has the greater influence on the component. For the upper slave link, it can be seen that the rotational motion caused by gear walking induces the primary loading on this component, whereas the lower slave link is affected by both gear walk and shimmy vibrational loading. This behavior could have been anticipated based of the joint definitions prescribed to each component; given that the lower slave link was connected through a ball joint on one end and a universal joint on the other, the increased degrees of freedom explains the greater amount of excitation.

In terms of structural behavior, a stress contour for the upper and lower slave link was plotted at the time-step when the maximum von Mises stress occurs. Additionally, another plot is generated to show a stress history for the element which experiences the highest stress of each component through the simulation. From the results, the highest stress occurs at 0.008 s, which corresponds to the first peak stress amplitude. Beyond this point, the stress continues to cycle and diminish.

5 Conceptual design

5.1 Design space generation

With the MBD analysis successfully implemented, the landing gear model is ready to be reconfigured to perform topology optimization. The first step is to generate a solid

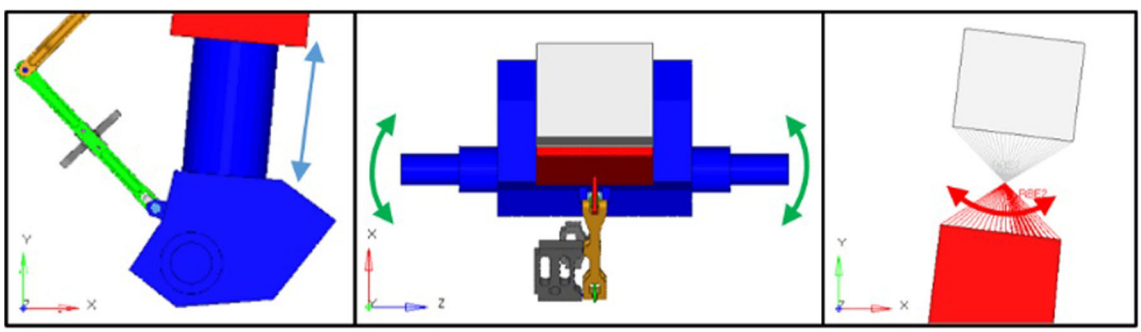

Fig. 5 Joint input motions for MBD

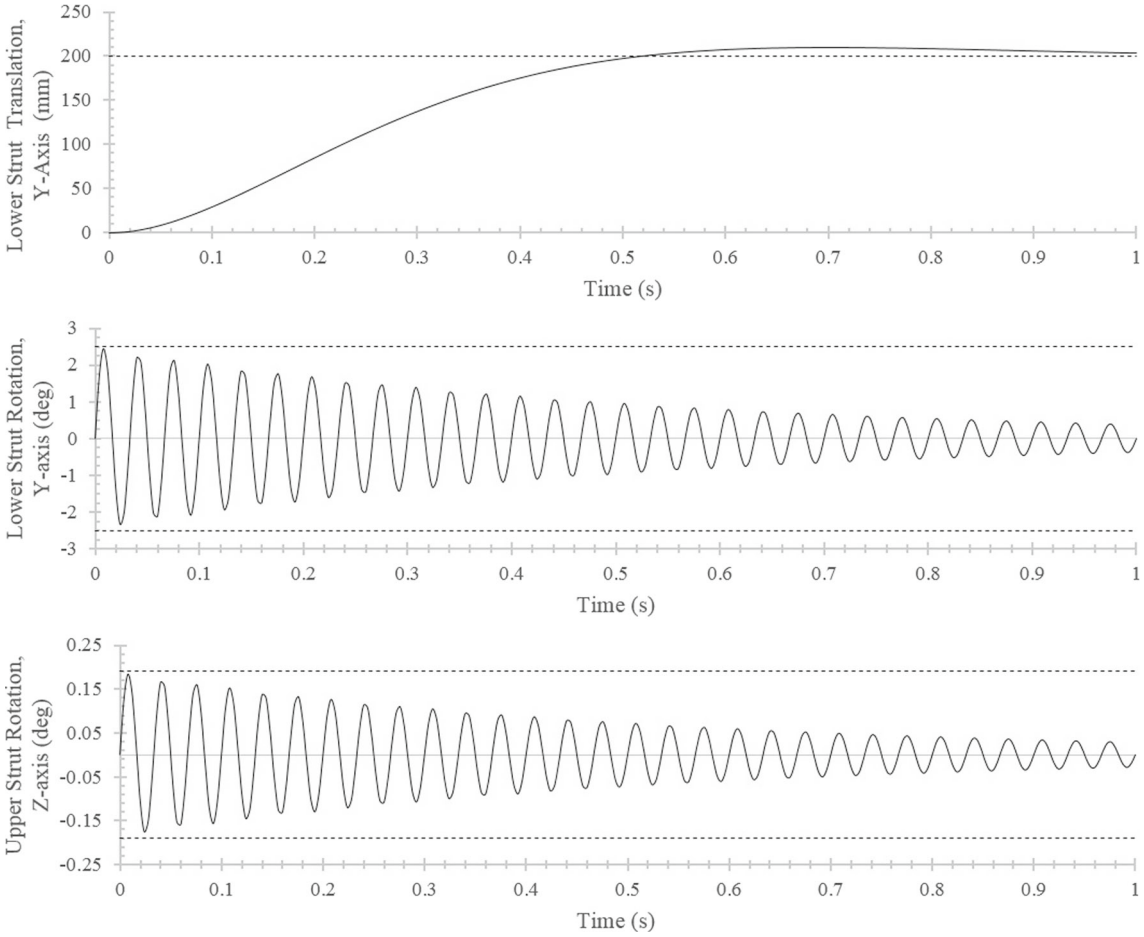

Fig. 6 Input motion functions for MBD analysis

design space based on the original upper and lower slave link CAD geometries by de-featuring the model to create a uniform domain.

Certain cutouts were left unchanged, in order to prevent interference between each component when loaded. Since there are various locations where connections have to be made to connect the design space to joints, a ring of elements was designated as a non-designable space, meaning these elements are not altered throughout the optimization. This ensures the joints are always properly connected to the component and prevent any numerical instabilities from occurring. The generated design spaces are shown in Fig. 7.

The upper slave link design space was segmented into two separate design spaces because preliminary topology

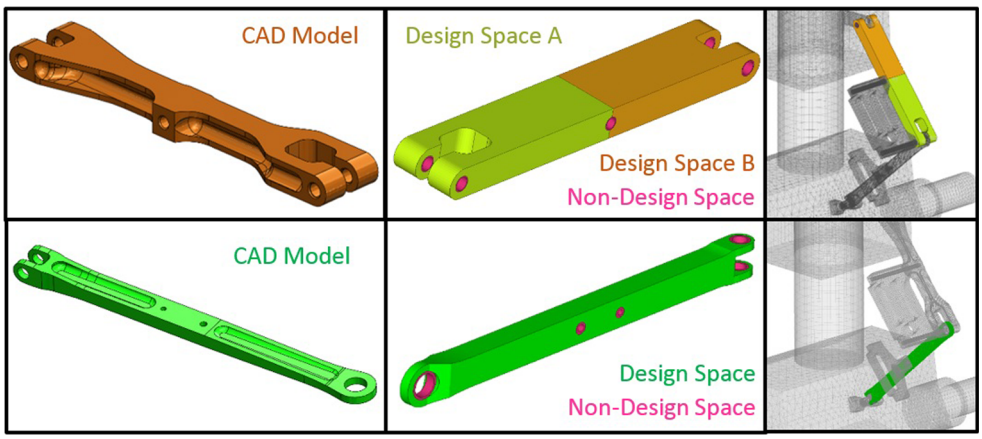

Fig. 7 Design space generation

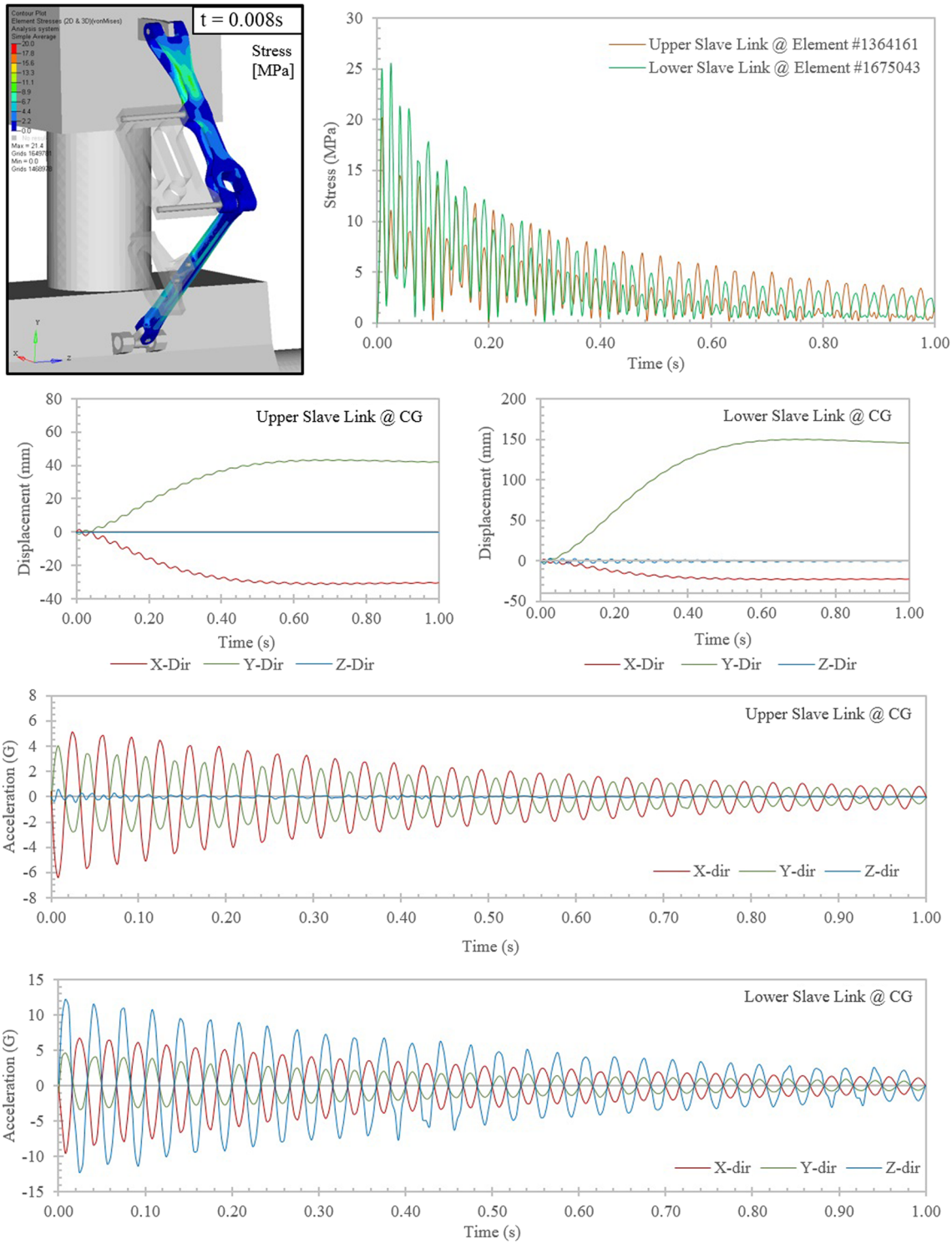

Fig. 8 Output from MBD analysis

optimization runs resulted in elements accumulating solely in design space B while design space A remained virtually void. Upon closer inspection, it was determined that the cause of this behavior was due to the difference in compliance caused by the presence of the upper cable guide. The stiffness from the cable guide was the reason that no solid elements were generated in design space A. Our solution to mitigate this phenomenon was to optimize with only one design space active at a time. This resolved the issue, and optimization parameters will be further discussed in the subsequent section.

5.2 Topology optimization

The objective function of the topology optimization is to minimize compliance under dynamic loading. The optimization algorithm chosen in Optistruct was a dual optimizer based on separable convex approximation. In order to translate a time-based response into multiple load cases for topology optimization, the equivalent static load method (ESLM) developed by Park and implemented in Optistruct 14.0 may be utilized. Park has published several papers that thoroughly explain the methodology (2011) and validations (Park & Kang 2003) performed on this technique. In essence, this process can be expressed mathematically in a simplified manner with the following equation:

$$f_{eq}^{t} = K_L(\rho_i)U_D(t) \tag{9}$$

where f_{eq}^{t} is the equivalent static loads vector at time step t, K_L is the linear global stiffness matrix, and U_D is the dynamic analysis displacement vector at time t.

For density-based topology optimization, solid isotropic microstructure penalization (SIMP) method, developed by Bendsøe and Sigmund (1999), is used to enhance the discretizing of the underlying relaxed mixed integer nonlinear problem (MINLP) and forcing intermediate element densities to converge towards either a 0 (void element) or 1 (solid element). This is done using the following penalization scheme:

$$E = \rho_i{}^{P} E_0 \tag{10}$$

where E represents the penalized Young's modulus of the i-th element, E_0 is the Young's modulus of the material, and P is the penalty factor. For all optimization runs, P is set to 3.

To drive the solution towards a feasible design, control parameters such as checkerboard and minimum member size filters (Zhou et al. 2001), manufacturing constraints and symmetry planes (Vatanabe et al. 2016). Multiple optimization runs were performed with different control parameter settings and volume fraction targets. To establish a baseline for comparison, a topology optimization run with no control parameters enabled was done for each design space. All topology optimization runs were conducted on a Windows workstation PC (Intel i7-5820 k, 12 cores 4.0 GHz, 65,431 MB DDR4 RAM 2133 MHz) and the CPU time for each run was recorded. These settings and CPU times are listed in Table 5. Figure 10 shows the results of each topology optimization run. A density threshold of 0.505 was set for the results of R1 to R3, and 0.755 for R4 to R9.

5.3 Optimization convergence

Once completed, objective values for compliance at every iteration were extracted from the output text files for each optimization run. Convergence plots were generated and shown in Fig. 9.

Without any manufacturing and symmetry constraints (R1, R4, and R7), the optimization converges relatively quickly and the profile is as one would expect. In the other optimization runs, there are three noticeable spikes in compliance followed by a gradual convergence at the end. This behavior is attributed to how OptiStruct handles and implements manufacturing and symmetry constraints.

As seen from the plots, a key difference of Topology Optimization with ELSM is the presence of outerloops (k). Since the loads experienced changes with the geometry of the structure, outerloops play a necessary step to recalculate the equivalent static loads of the updated geometry for improved accuracy in the optimization. The effectiveness of this approach is seen in the abrupt change in compliance that is typically observed during the transition from outerloop 1 to 2. Another interesting trend to note is that the transition of subsequent outerloops is typically smooth, which may suggest the structure is not changing drastically and, as a result, not changing the recalculated loads by a noticeable amount.

Table 5 Optimization parameters, settings, and computational cost

Design Space	Run ID	Volume Fraction	Manufacturing Constraint	Symmetry Constraint	Minimum Member Size	CPU Time (hour)	MBD ESLM Outerloops (k)	Number of Iterations
Upper Slave Link (A)	R1	0.20	N/A	N/A	N/A	15.70	4	41
	R2	0.20	Split Draw	1 plane	3	30.30	4	73
	R3	0.20	Split Draw	2 plane	3	27.13	4	76
Upper Slave Link (B)	R4	0.20	N/A	N/A	N/A	19.30	4	37
	R5	0.20	Split Draw	1 plane	3	56.75	5	92
	R6	0.20	Split Draw	2 plane	3	46.12	6	106
Lower Slave Link	R7	0.25	N/A	N/A	N/A	7.92	4	41
	R8	0.20	Split Draw	1 plane	3	10.18	3	55
	R9	0.25	Split Draw	2 plane	3	13.43	3	55

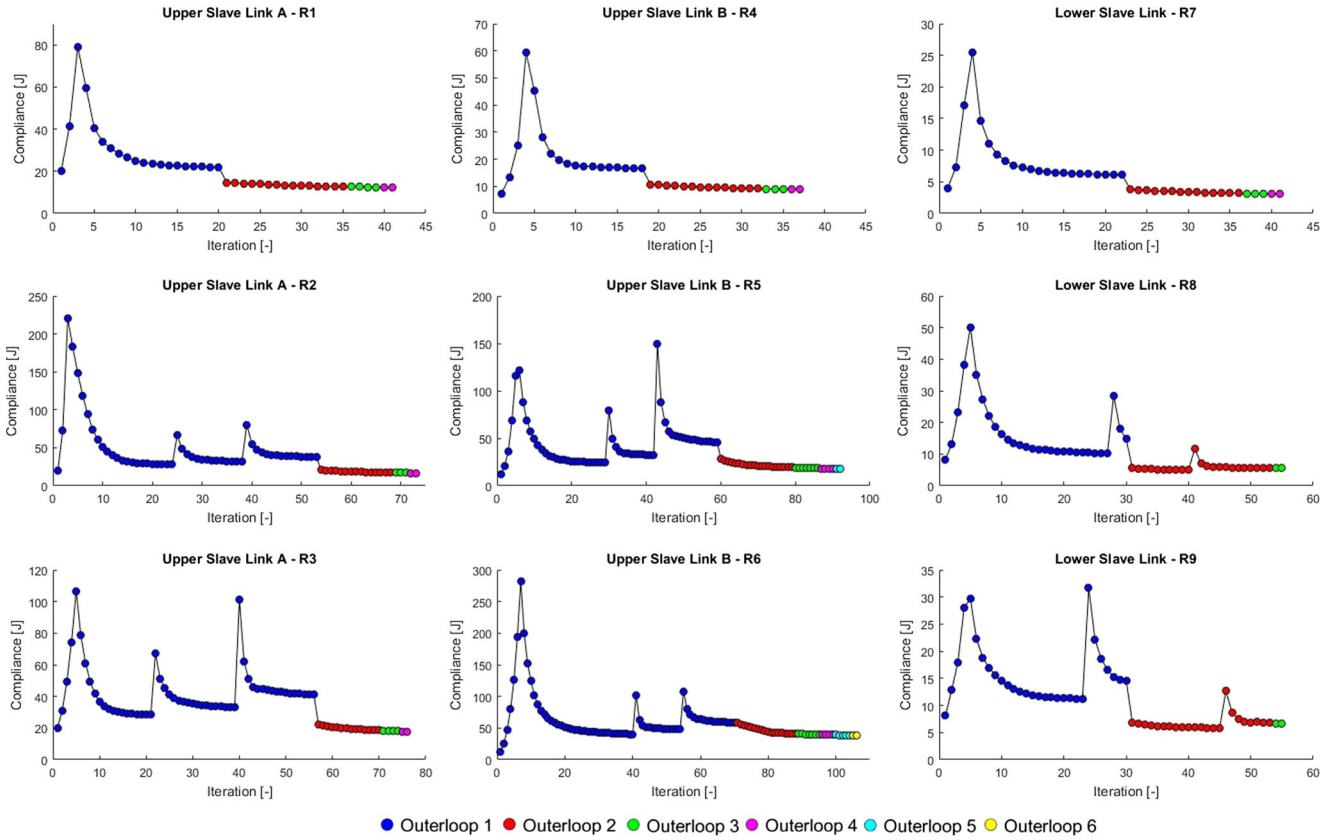

Fig. 9 Optimization convergence plots

6 Detailed design

6.1 Topology result interpretation

Based on the findings from multiple topology optimization results from Fig. 10, there are certain commonalities and differences that can be used towards developing an optimal design. In runs where no manufacturing or symmetry constraints were imposed (R1, R4 and R7), the structures formed have an organic nature in their formation, with no clear method for reproducing the results with traditional manufacturing techniques. Another interesting behavior exhibited by these results is that areas of high densities typically occurs near the boundary of the design space.

For results in R2, R5, and R8, a split draw manufacturing constraint and single plane of symmetry was activated during these runs, which shows some promising insights. All results exhibited a hollow structure behavior; however, R2 and R8 also show resemblances of truss structures and cutouts.

Lastly, in runs R3, R6, and R9, a split draw constraint along with 2 planes of symmetry were used to constrain the design space towards a feasible design. Again, the results followed a hollow structure behavior, but the distribution of cutouts and truss structures did change in terms location, size, and shape.

To realize and validate the results of topology optimization under dynamic loading, isosurfaces from runs R2, R6, and R8 were chosen as the template to be used to generate revised designs.

6.2 Revised design generation

Once the isosurfaces were selected, STL files were generated and exported to a CAD modeling software program. In order to have a better visualization of the boundaries of the design space as well as to ensure the pinhole locations of the revised design match the existing baseline, the imported iso-surfaces were projected onto the CAD model of the design space for both upper and lower slave link.

Two different approaches were taken when generating designs from the topology isosurfaces. The first approach (Revised Design #1) involved trying to replicate as many of the features present in the topology results as possible with little consideration of manufacturability. Therefore, a design based upon the use of rectangular tubing, bushing inserts, laser cutting, and sheet metal operations as the manufacturing inspiration was created. Bushings are used in areas where pins are to be inserted, as they will increase the contact area. Although it is possible to manufacture this design with current and existing manufacturing methods, it would likely be infeasible due to the high degree of complexity and cost associated with producing such a component. Nonetheless, this design was produced to demonstrate the full and potential benefits in

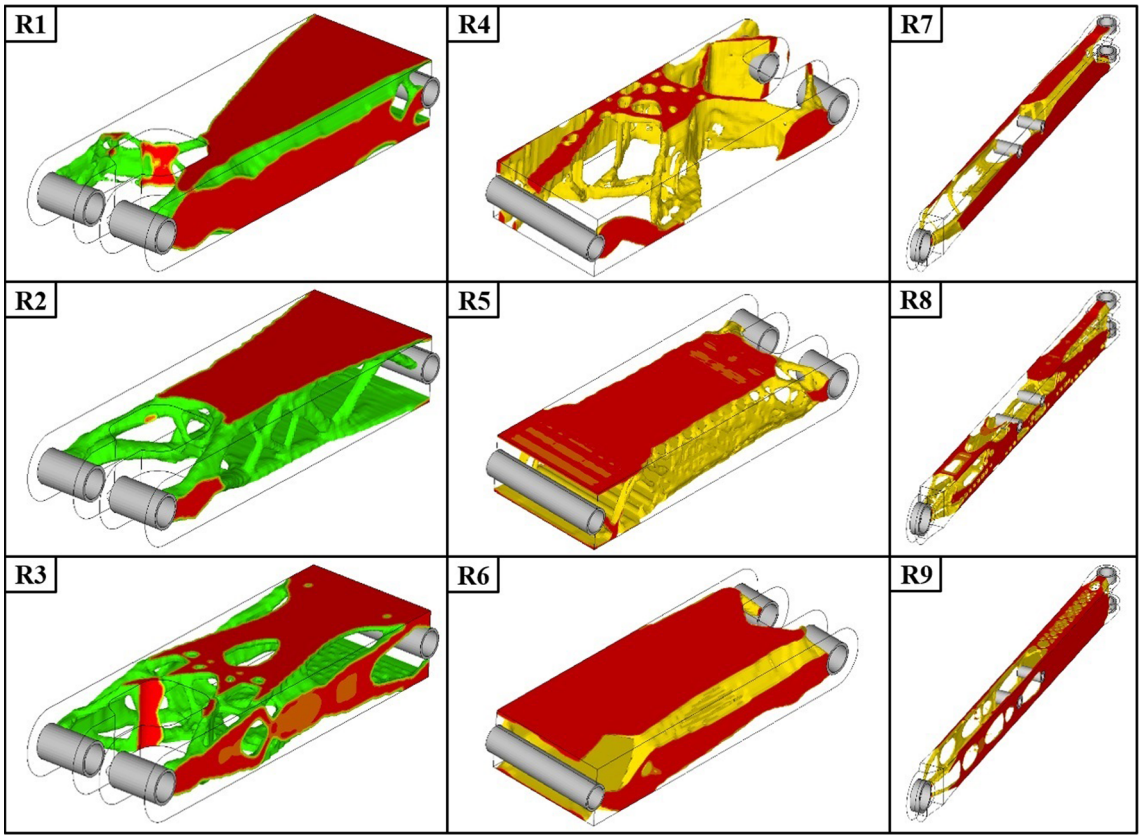

Fig. 10 Topology optimization results for upper slave link design space A (R1-R3), Upper Slave Link Design Space B (R4-R6), and Lower Slave Link (R7-R9). Optimization parameters used for each result is summarized in Table 5

terms of weight and performance that can achieved directly from the raw topology results.

The second approach (Revised Design #2) in design generation created a design that improves on the manufacturability and cost savings of the baseline design. Currently, the baseline design is manufactured using CNC milling of a block of aluminum with several drilling, pocketing, and facing operations. Constrained by manufacturing operations of CNC milling, the generated designs had to deviate from the isosurfaces of the topology results. In order to introduce both weight and cost savings with current manufacturing methods, Revised Design #2 was created with fewer machining operations and a smaller stock aluminum volume.

The revised designs for both the upper and lower slave link are shown in Figs. 11 and 12. Compared with the baseline the design, Revised Design #1 yield weight savings of 60% and 70%, for the upper and lower slave link, respectively and Revised Design #2 yield weight savings of 41% and 24%.

7 Design validation

The CAD model of the revised designs were exported and brought into the MBD finite element model for a comparative analysis, with respect to the baseline design. After re-meshing and ensuring all joints were properly defined and connected, MBD analysis was performed for both Revised Designs #1 and #2, and the results are shown in Fig. 13.

In Fig. 13, the stress versus time plot shows an increased amount of stress experienced at the peaks of each cycle by Revised Design #1. For the upper slave link, the peak stress occurs at 0.008 s, increases by 74% (35 MPa) from the baseline, while the lower slave link experiences a 68% (42 MPa) increase. An increase in stress is typically observed when weight savings are applied to a component; however, Revised Design #2 shows that it is possible to obtain weight savings without significant changes to the structural performance of the system. For Revised Design #2, a 6% increase in peak stress was observed for the upper slave link and a 14% decrease in stress for the lower slave link (Table 6).

In order to compare the dynamic performance, MBD results for both revised designs are generated and shown in Fig. 14. It can be see the displacement and acceleration contours do not significantly differ from the baseline in Fig. 8. Components in Revised Design #1 do see slightly lower acceleration values in the Z-direction, relative to Revised Design #2, which may be attributed to the lighter design contributing less inertial loading and added double shear joint in the

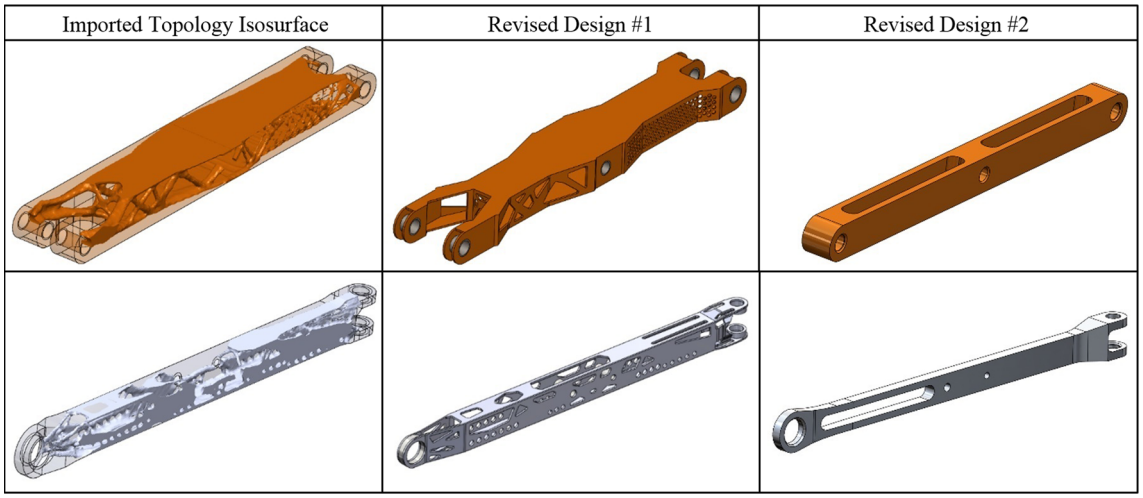

Fig. 11 Revised design interpreted from topology results

geometry of the upper slave link in #1 versus the single shear joint in #2. Despite slightly lower acceleration values, #1 still sees higher stresses than #2, as seen in Fig. 13.

The peak stresses for Revised Design #1 were identified to occur in localized areas where cutouts or weight savings measures have been implemented (Fig. 12). For the upper slave link, the high stresses occur in the perforated areas near the revolute joint (B), while the lower slave link experiences stress concentrations in a fillet close to the revolute joint (A). To reduce these peak stresses without significant impact on weight savings, size and shape optimization could be done as a subsequent step to refine certain features in the design and eliminate stress concentrations.

From Table 1, the increased peak stress from the revised designs are still well below the yield strength of the material (436 MPa). Nevertheless, it is important to note that since these components are subjected to a high frequency vibrational load, failure over time due to fatigue is more prevalent and likely situation. Based on fatigue characteristics for Al − 7075 identified by Tanaka et al. (1984), the stresses experienced by the revised designs were still well below the fatigue limit (approximately 150 MPa). For this reason, fatigue analysis

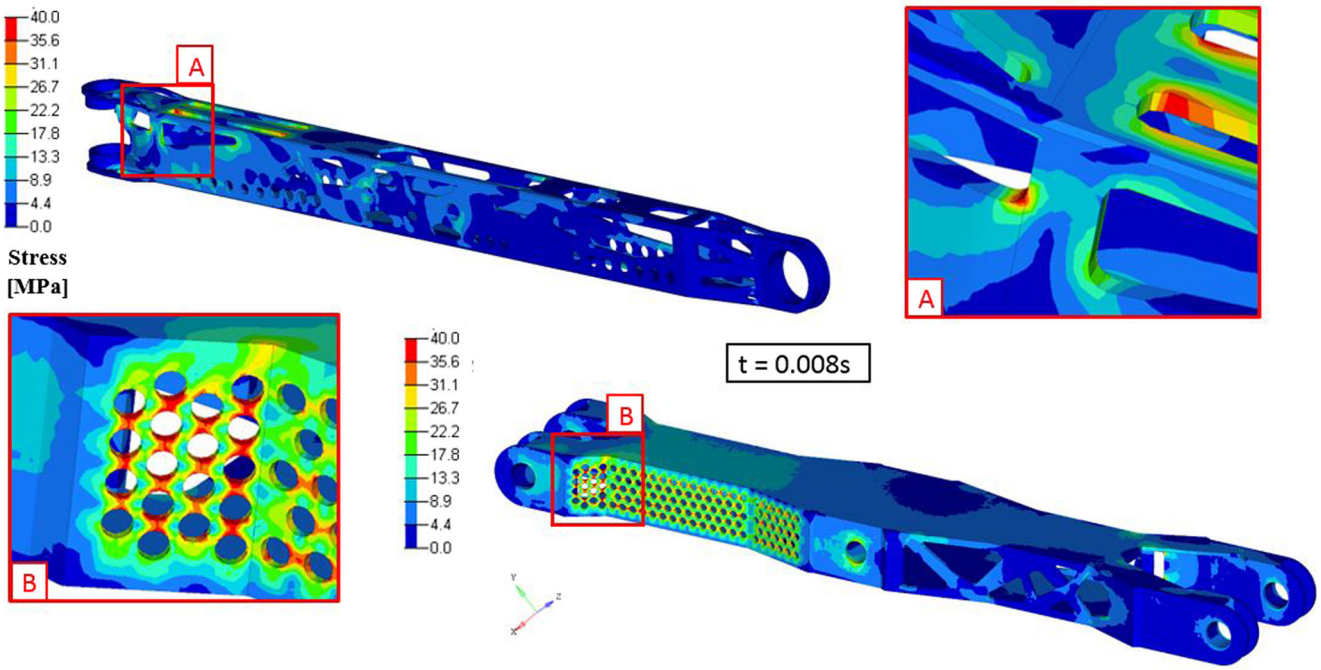

Fig. 12 Areas of high stress for revised design #1

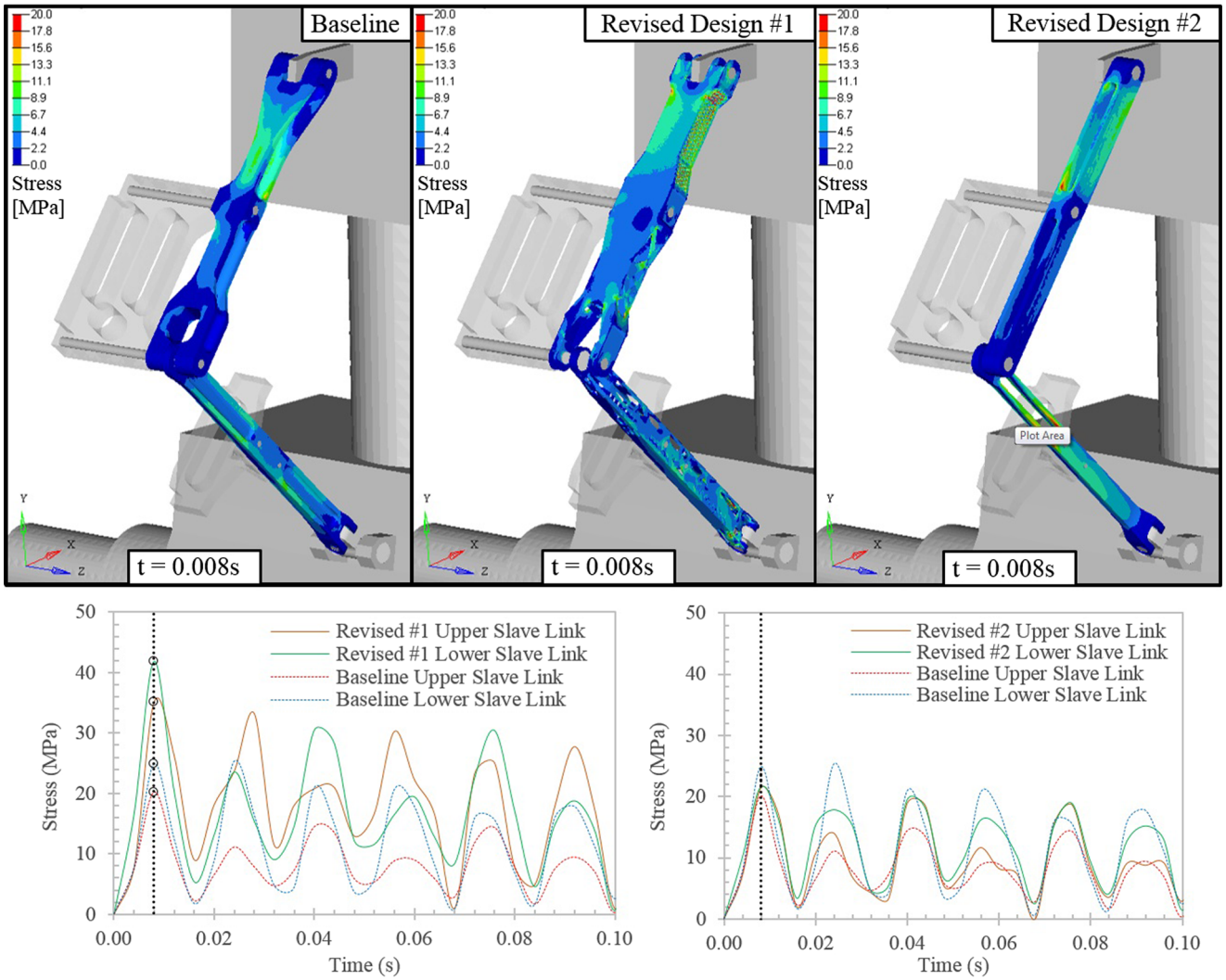

Fig. 13 Output from MBD analysis for revised components. As shown from the stress plots, Revised Design #1 (Left) experiences higher stresses than Revised Design #2 (Right) during a single landing cycle

was not conducted during the design validation, as the peak stresses would not lead to any considerable amount of damage in these components.

Although not performed in this study, it should be noted that the results generated from MBD analysis has the potential to be directly utilized in a fatigue analysis. Dynamic load history containing stress and strain data over time may be readily exported from the MBD analysis and into a fatigue analysis software program such as nCode Design Life. The first advantage to this is the additional post-processing and computational resources required to export these results are minimal. Since the load history is extracted directly from the MBD analysis and not an artificially scaled static load history, the results produced by the fatigue analysis also has the potential to be more accurate, assuming the simulated conditions closely match the physical system.

Table 6 Performance metrics of revised designs

Component	Weight Savings	Peak Stress
Revised Design #1		
Upper Slave Link	-70%	+74%
Lower Slave Link	−60%	+68%
Overall	−67%	–
Revised Design #2		
Upper Slave Link	−41%	+6%
Lower Slave Link	−24%	−14%
Overall	−36%	–

8 Limitations

In our paper, three main limitations need to be addressed and justified. The first involves the manufacturability of Revised Design #1; the second is related to topology optimization for

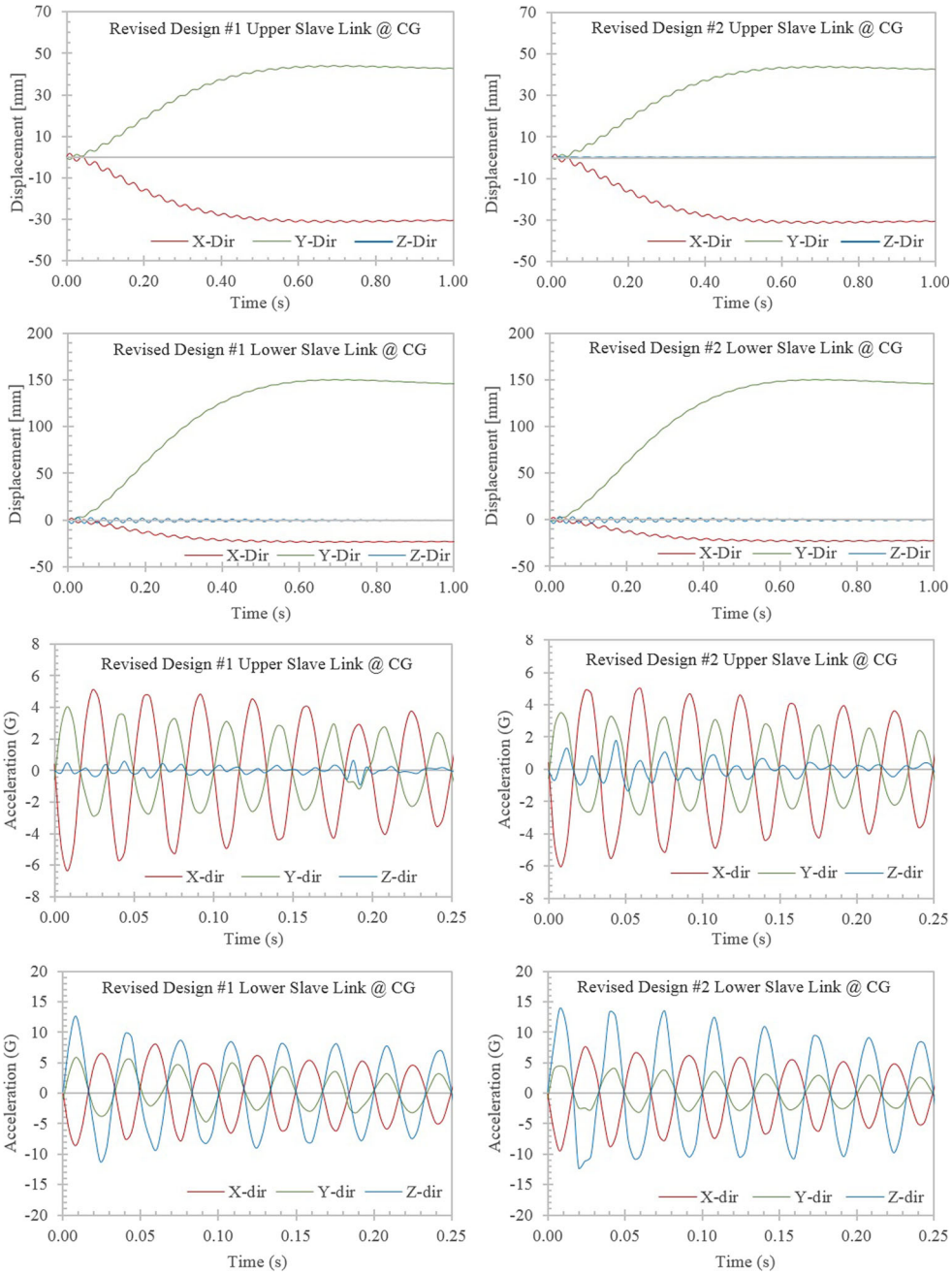

Fig. 14 Displacement and acceleration plots from MBD Analysis of Revised Design #1 and #2

manufacturing cost, and the third being the lack of shape and size optimization following the generation of the revised designs.

While manufacturability, cost savings, and shape/size optimization are important to consider rigorously in typical design practice, the emphasis put on this paper was on demonstrating an approach that has been verified in simple cases can also be applied to geometries with greater complexity while being able to achieve similar benefits.

It can be argued that certain features in Revised Design #1 are either impractical or infeasible to manufacture and design modifications would need to be made in order to accommodate tooling and equipment availability. These modifications would tend to sacrifice weight savings of the optimized design; however, this should be identified as a limitation of the current manufacturing technologies available rather than a limitation of the approach's capabilities. As new techniques such as additive manufacturing begin to mature and become a feasible option, manufacturing limitations will be reduced and a completely new bound of methods would emerge for reinterpreting the topology results for design generation.

Cost savings was another aspect that was not thoroughly explored due to the complexities that come with incorporating

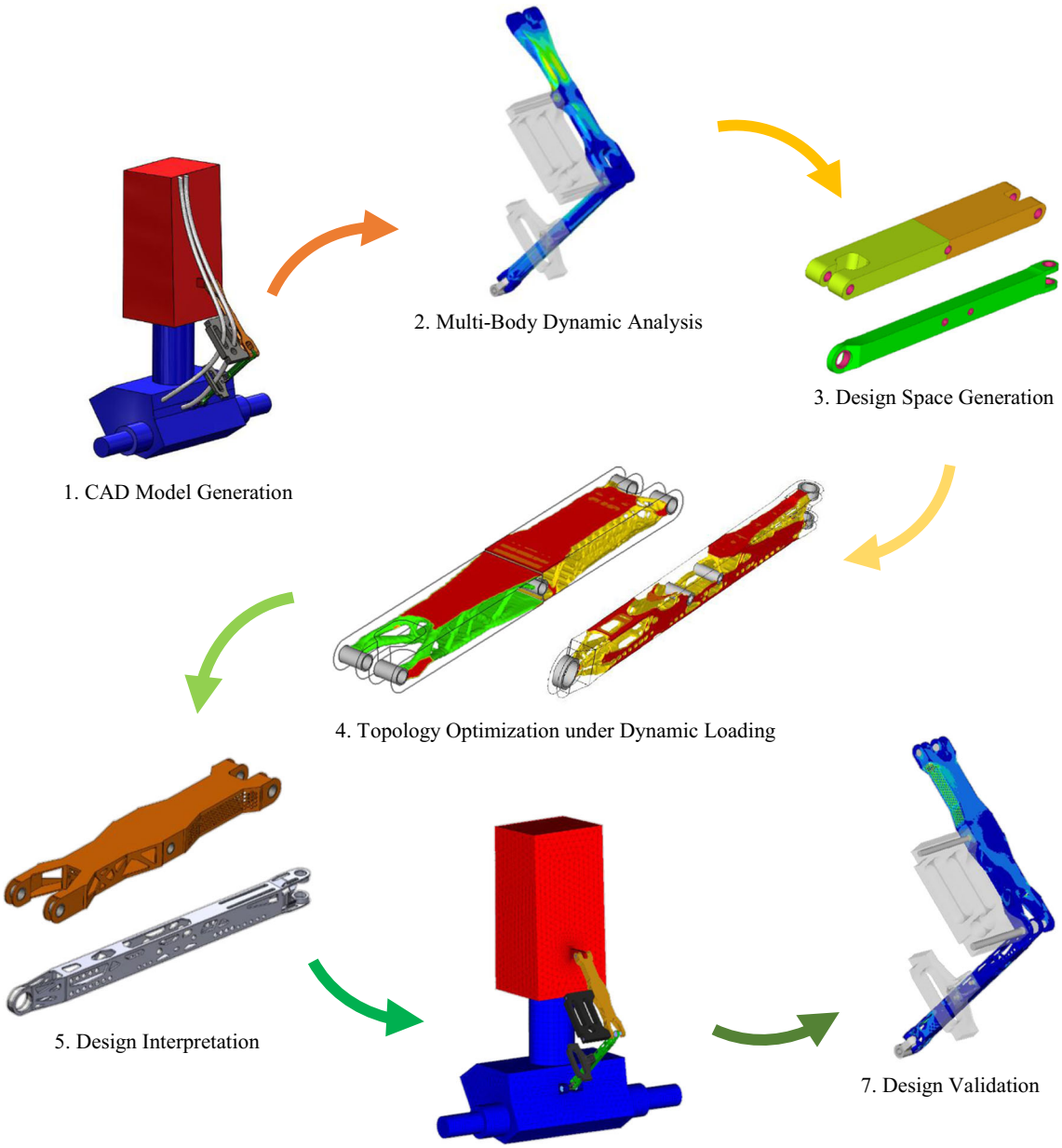

Fig. 15 Slave link assembly design optimization process overview

an accurate and objective mathematical cost model into the optimization problem statement. The root of these complexities comes from the variability in the cost model depending on which manufacturing process is utilized to develop the design. Additionally, uncertainty within these manufacturing processes are also present as the cost model changes depending on the type and capacity of facilities and equipment available as well as the various possible permutations of machining operations that may be used to create the same component. The industrial partner, Safran Landing Systems, utilized internal costing metrics and estimated the cost savings for Revised Design #2 to be 60%, relative to the baseline.

For a similar reason, size and shape optimization was not performed because the amount of weight savings these stages of optimization will introduce to a design is significantly less than the potential weight savings that can be realized through topology optimization under dynamic loading. Given the nature of the ESLM formulation, size and shape optimization under dynamic loading for complex structures can also be considered, however the results are highly dependent and limited by the geometry of the component.

The objective of this paper was to demonstrate the potentials of incorporating the approach of using MBD analysis and topology optimization with ESLM for aircraft landing gear

assemblies, which undergo complex dynamic loading. Although manufacturability and shape/size optimization were not extensively covered, these items will be important to explore into details as this approach is adopted into modern design practices. If implemented, the approach has the prospect of realizing additional cost and weight savings.

9 Conclusion

This paper has shown an effective and efficient approach to model, analyze, optimize, and validate landing gear assembly components such as the slave link mechanism while considering a realistic dynamic loading scenarios and modeling the parts as deformable bodies. Fig. 15 shows an overview of the entire design process undertaken. An initial design domain was generated based off features from the original slave link designs. Dynamic loading topology optimization runs were then performed on each component with various control parameters enabled in order to obtain a variety of optimal solutions. Iso-surfaces were obtained from certain results and used to generate two revised and lightweight designs. The new designs were validated using the same model used to analyze the baseline design. Finally, it was determined that the revised designs were in fact able to perform as intended.

It should be made clear that the problem statement of the optimization does not encompass all possible failure modes, such as buckling, damage at the joints, and degradation of material properties. From the view point of uncertainties, this work is a deterministic optimization, and therefore it should be a first step to robust design practices. Optimization with the consideration of variations should be taken into consideration as future work: variations in material properties, manufacturing operations, and operation.

Compared to traditional modeling and optimization approaches for dynamic systems, this approach shows great potential for shortening product development cycles. Rather than performing manual translations of dynamic reaction forces that are dependent on the geometry into multiple static load cases for optimization, the utilization of ESLM for MBD analysis can enable users to perform this task efficiently. These time benefits can also be seen during the validation process, where new components can simply be swapped into an existing MBD model and analyzed with minimal user inputs. Analogous with being a virtual test rig, another benefit that is gained from this approach is the ability to save costs in prototype iterations. The efficiency in setup and running multiple analysis with different designs helps identify and mitigate the risk of design flaws before physical testing and validation. As the aerospace industry continues to increase their weight and cost targets within aggressive timelines, approaches and design processes such as the one presented in this research will inevitably have to be adopted to other components and subsystems in order to ensure that these future targets are achieved.

Acknowledgements The authors would like to express their gratitude to Joseph Lan and James Ning at Safran Landing Systems Canada for their expertise and guidance throughout the course of this research. This research was supported by the National Science and Engineering Research Council of Canada and Safran Landing Systems Canada. The contributions made are greatly appreciated.

References

AGARD Report (1995) The design, qualification and maintenance of vibration-free landing gear (R-800)

Altair OptiStruct (2015a) OptiStruct 14.0 Reference Guide. Altair Engineering, Inc., Troy

Altair OptiStruct (2015b) MotionSolve 14.0 reference guide. Altair Engineering, Inc., Troy

Bauchau OA (2011) Flexible Multibody Dynamics. Springer Netherlands, Atlanta, GA

Bendsøe MP, Sigmund O (1999) Material interpolation schemes in topology optimization. Arch Appl Mech 69:635–654. https://doi.org/10.1007/s004190050248

Besselink IJM (2000) Shimmy of Aircraft Main Landing Gears. Delft University of Technology, Delft, Netherlands

Brenan KE, Campbell SLV, Petzold LR (1996) Numerical solution of initial-value problems in differential-algebraic equations. Book 256

Cardona A (2000) Superelements modelling in flexible multibody dynamics. Multibody Syst Dyn 4:245–266. https://doi.org/10.1023/A:1009875930

Choi WS, Park KB, Park GJ (2005) Calculation of equivalent static loads and its application. Nucl Eng Des 235:2337–2348. https://doi.org/10.1016/j.nucengdes.2005.05.030

Craig RR, Bampton MCC (1968) Coupling of substructure for dynamic analyses. AIAA J 6:1313–1319

Denti E, Fanteria D (2010) Models of Wheel Contact Dynamics : An Analytical Study on the In-Plane Transient Responses of a Brush Model. Veh Syst Dyn 34:37–41

Deveau S (2013) Transportation - should Airlines start charging by the pound. Financ. Post

DuPont (2016) Acetal Resin DuPont™ Delrin ® 100 NC010

Engineering A (2008) Multi-disciplinary design of an aircraft landing gear with altair hyperworks altair engineering, October 2008

Gowda AC, Basha N (2014) Trends in mechanical engineering & technology linear static and fatigue analysis of nose landing gear for trainer aircraft. 4:1–10

Hitch HPY (1981) Aircraft ground dynamics. Veh Syst Dyn 10:319–332. https://doi.org/10.1080/00423118108968681

International Air Transport Association (2016a) IATA forecasts passenger demand to double over 20 Years. IATA Press Release No 59 18–22

International Air Transport Association (2016b) Fact Sheet : Climate Change. IATA Environ. Policy 1–3

Kang BS, Choi WS, Park GJ (2001) Structural optimization under equivalent static loads transformed from dynamic loads based on displacement. Comput Struct 79:145–154. https://doi.org/10.1016/S0045-7949(00)00127-9

Knowles JAC, Krauskopf B, Lowenberg M (2013) Numerical continuation analysis of a three-dimensional aircraft main landing gear mechanism. Nonlinear Dyn 71:331–352. https://doi.org/10.1007/s11071-012-0664-z

Krüger WR, Morandini M (2014) Recent developments at the numerical simulation of landing gear dynamics. CEAS Aeronaut J 1:55–68. https://doi.org/10.1007/s13272-011-0003-y

Krüger WR, Besselink IJM, Cowling D et al (1997) Aircraft landing gear dynamics: simulation and control. Veh Syst Dyn 28:119–158. https://doi.org/10.1080/00423119708969352

Lee HA, Park GJ (2012) Topology optimization for structures with nonlinear behavior using the equivalent static loads method. J Mech Des 134:14. https://doi.org/10.1115/1.4005600

Li M, Tang W, Yuan M (2014) Structural dynamic topology optimization based on dynamic reliability using equivalent static loads. Struct Multidiscip Optim 49:121–129. https://doi.org/10.1007/s00158-013-0965-y

Nguyen T, Schonning A, Eason P, Nicholson D (2012) Methods for analyzing nose gear during landing using structural finite element analysis. J Aircr 49:275–280. https://doi.org/10.2514/1.C031519

Oh SH (2014) A study on development of dual locking linkage for landing gear for the application to UAV. 7:41–48

Park GJ (2011) Technical overview of the equivalent static loads method for non-linear static response structural optimization. Struct Multidiscip Optim 43:319–337. https://doi.org/10.1007/s00158-010-0530-x

Park GJ, Kang BS (2003) Validation of a structural optimization algorithm transforming dynamic loads into equivalent static loads. J Optim Theory Appl 118:191–200. https://doi.org/10.1023/A:1024799727258

Pritchard J (2001) Overview of landing gear dynamics. J Aircr 38:130–137. https://doi.org/10.2514/2.2744

Schmidt M, Rohrbach K (1990) ASM handbook, volume 1: properties and selection: irons, steels, and high-performance alloys. Met Handb 1:793–800. https://doi.org/10.1361/asmhba0001

Shabana AA (1997) Flexible multibody dynamics: review of past and recent developments. Multibody Syst Dyn 1:189–222. https://doi.org/10.1023/A1009773505418

Sun J, Tian Q, Hu H (2016) Structural optimization of flexible components in a flexible multibody system modeled via ANCF. Mech Mach Theory 104:59–80. https://doi.org/10.1016/j.mechmachtheory.2016.05.008

Tadeusz N, Jerzy M, Adam B (2006) Numerical analysis of a front support landing gear dynamics. 3–10

Tanaka K, Matsuoka S, Kimura M (1984) Fatigue Strength of 7075-T6 Aluminium Alloy Under Combined Axial Loading and Torsion. Fatigue Fract Eng Mater Struct 7:195–211. https://doi.org/10.1111/j.1460-2695.1984.tb00189.x

Vatanabe SL, Lippi TN, de Lima CR et al (2016) Topology optimization with manufacturing constraints: a unified projection-based approach. Adv Eng Softw 100:97–112. https://doi.org/10.1016/j.advengsoft.2016.07.002

Xingguo M, Xiaomei Y, Bangchun W (2007) Multi-body dynamics simulation on flexible crankshaft system. 12th IFTOMM World Congr World Congr 3–5

Zhou M, Shyy YK, Thomas HL (2001) Checkerboard and minimum member size control in topology optimization. Struct Multidiscip Optim 21:152–158. https://doi.org/10.1007/s001580050179